coatings

MDPI

Article

Investigations of TiO_2/NanoTiO_2 Bimodal Coatings Obtained by a Hybrid PVD/ALD Method on Al-Si-Cu Alloy Substrate

Marcin Staszuk [1,*], Łukasz Reimann [2], Daniel Pakuła [1], Mirosława Pawlyta [2], Małgorzata Musztyfaga-Staszuk [3], Paweł Czaja [4] and Petr Beneš [5]

1 Department of Engineering Materials and Biomaterials, Silesian University of Technology, Konarskiego St. 18a, 44-100 Gliwice, Poland; daniel.pakula@polsl.pl
2 Materials Research Laboratory, Silesian University of Technology, Konarskiego St. 18a, 44-100 Gliwice, Poland; lukasz.reimann@polsl.pl (Ł.R.); miroslawa.pawlyta@polsl.pl (M.P.)
3 Welding Department, Silesian University of Technology, Konarskiego St. 18a, 44-100 Gliwice, Poland; malgorzata.musztyfaga-staszuk@polsl.pl
4 Institute of Metallurgy and Materials Science, Polish Academy of Sciences, 25 Reymonta St., 30-059 Krakow, Poland; p.czaja@imim.pl
5 Department of Material Science and Technology, University of West Bohemia, Univerzitní 22, 301 00 Pilsen, Czech Republic; pbenes@kmm.zcu.cz
* Correspondence: marcin.staszuk@polsl.pl

Abstract: This study aimed to investigate the influence of bimodal TiO_2/nanoTiO_2 coatings obtained in the PVD/ALD hybrid process on an Al-Si-Cu-type aluminium alloy on the physicochemical properties of the investigated materials. The reference materials were uncoated substrates and samples coated with TiO_2 coatings in single PVD and ALD processes. Tests were carried out on the morphology of coatings using scanning electron microscopy (SEM) and atomic force microscopy (AFM) to determine the structure of the tested coatings and their influence on physicochemical properties. The tests of physicochemical properties were carried out using the potentiodynamic and electrochemical impedance spectroscopy methods. The analysis of corrosion products obtained during the study of physicochemical properties was performed using SEM and EDS analysis. Based on the analysis of anode polarisation curves of the tested materials and Tafel analysis, it was found that a sample demonstrated the highest corrosion resistance with a bimodal coating-type TiO_2/nanoTiO_2, which had the lowest value of corrosion current and the highest value of polarisation resistance. The slightest corrosion resistance was characteristic for uncovered samples. Moreover, the influence of the tested coatings on the improvement of tribological contact of the surfaces of the coated materials with the counter-specimen made of cemented carbides was demonstrated.

Keywords: PVD; ALD; hybrid coatings; aluminium alloys; corrosion resistance; tribology; titanium oxide; TiO_2

Citation: Staszuk, M.; Reimann, Ł.; Pakuła, D.; Pawlyta, M.; Musztyfaga-Staszuk, M.; Czaja, P.; Beneš, P. Investigations of TiO_2/NanoTiO_2 Bimodal Coatings Obtained by a Hybrid PVD/ALD Method on Al-Si-Cu Alloy Substrate. *Coatings* **2022**, *12*, 338. https://doi.org/10.3390/coatings12030338

Academic Editor: Lech Pawlowski

Received: 28 December 2021
Accepted: 1 March 2022
Published: 4 March 2022

1. Introduction

For many years, multi-component aluminium alloys (including Al-Si-Cu alloy) have been widely used, primarily in the machinery, armaments, aviation, and automotive industries. These alloys are characterised by castability, good electrical and thermal conductivity, and giving way to strength properties. Unfortunately, in the three-component Al-Si-Cu alloys, the addition of copper facilitating their heat treatment affects the deterioration of corrosion resistance. Moreover, the disadvantage of these alloys is also their low hardness. It is associated with low abrasion resistance. Solutions are being sought in surface treatment methods to eliminate problems with the unsatisfactory performance of these materials, in particular with reduced corrosion resistance. The studies published in the literature on the surface treatment of silumin show that the most promising are coatings obtained by physical vapour deposition techniques (PVD) and plasma-assisted chemical vapour

deposition (PACVD). In addition to PACVD, many research results also concern using the latest atomic deposition technique of ALD coatings. Coatings obtained as a result of the synergy of the interaction of hybrid surface treatment with the use of PVD and ALD techniques are increasingly of particular interest [1–20].

In their works, the authors showed the improvement of the functional properties of the tested materials using the following coating materials: Cr/CrN/CrN, Cr/CrN/TiN, Ti/Ti(C,N)/CrN, Ti/Ti(C,N)/(Ti,Al)N, and Ti/(Ti,Si)N/(Ti,Si)N, obtained by the PVD method, and Ti/DLC/DLC obtained by the PACVD method. On the other hand, in the case of the ALD technique, very high corrosion resistance is provided by the TiO_2 phase. This was confirmed in numerous studies by coating it on stainless steel, among others. Moreover, this phase is characterised by a high refractive index, high electrical transmittance, and high stability [8–19]. The properties of TiO_2 coatings produced by the ALD method are strongly related to the parameters of the application process (coating growth temperature, applied precursors, number of cycles). Therefore, their selection is important [9,17,21–25]. TiO_2 coatings applied at temperatures below 200 °C show an amorphous structure, anatase and brookite are observed at temperatures between 200 and 500 °C, and rutile above 400 °C [21]. Controlling the process parameters makes it possible to influence the formation of individual phases of titanium dioxide, which in turn affects the properties of the coating that will be obtained and the possibilities of their applications. The adhesive properties of TiO_2 coatings are significantly influenced by the temperature and the number of deposition cycles. By changing the temperature of the TiO_2 coating deposition process, as was presented in [9], the best adhesive properties are demonstrated by coatings applied at a temperature of about 300 °C. In the selected studies, a certain tendency can also be noticed. On the one hand, the adhesive properties increase with the increasing process temperature, and on the other hand, the adhesive properties deteriorate significantly after exceeding a certain temperature. Different structures can be obtained by controlling the number of cycles during the application of the coatings. There is a general tendency for the amorphous structure to prevail for a small number of cycles. However, as the number of cycles increases, more readings of the crystalline phase are obtained [17]. The studies presented in [17] for 500 cycles showed the presence of anatase with an orientation of (211). As the number of cycles increased, more indications of crystal structure with the preferred orientation of (101) were noted. When the temperature changes, there is a similar relationship. With increasing temperature, the amorphous phase turns into a crystalline phase. Chung [22] noted an amorphous structure at a temperature of 182 °C, while at 236 °C, indications from the crystalline phase (anatase) began to appear. For temperatures of 236, 263, 291, and 318 °C, the tests showed the presence of anatase crystalline phase with the preferred orientation of (101). For a temperature of 345 °C, the orientation indications of (101) were recorded but were less distinct.

The work in [22] also presents the results of the AFM study, which showed a uniform surface at the temperature of 182 °C, characteristic for the amorphous structure for higher temperatures at the surface corresponding to the crystal structure, but above the temperature of 300 °C, it was again more uniform. Moreover, no indications of the crystalline phase were noted (XRD for the thinnest coatings), which indicates an amorphous state, while the coatings in which crystalline phase was detected were in each case about 2 µm thicker than the amorphous ones. The authors of [22] claim that such a phenomenon indicates a quick crystallisation from a specific layer thickness. The research also showed the following relationship: the critical thickness (at which the crystalline phase began to appear) and the size of the crystals decreased with the increasing temperature.

In turn, in [20], an attempt was made to improve the functional properties of the Al-Si-Cu alloy by depositing ALD + PVD hybrid coatings (ALD at the substrate). Unfortunately, corrosion tests have shown that the hybrid coating made in this way does not have better corrosion resistance than the PVD coating itself. Moreover, it does not even perform better than the uncoated substrate. Structure studies using the transmission electron microscope showed that there is no ALD coating under the PVD coating. These results showed that the

ALD coating degrades the PVD coatings during deposition. It was undoubtedly related to the atomisation phenomenon: the ALD layer was sprayed from the substrate with high-energy ions of the elements forming the PVD coating.

We can obtain excellent anti-corrosion properties using a combination of PVD/ALD coatings, as was confirmed by works from recent years. These properties are better than when using each of these techniques individually. In this hybrid system, the ALD layer seals the PVD layer, which is often defective due to its specific structure. In the combinations of CrN-Al_2O_3/TiO_2 and TiAlN/TiN/Al_2O_3, TiCN/Al_2O_3 coatings obtained on steels, in which the Al_2O_3 and TiO_2 phases are obtained by the ALD technique [26–33], take on the role of a sealant to provide very good corrosion resistance properties.

As shown by the first studies of the authors of this paper, excellent results are also achieved by applying a hybrid PVD/ALD coating [33] consisting of the same phases, called a bimodal coating. It has already been shown that the application of the bimodal PVD/ALD TiO_2/nanoTiO_2 coating on a stainless-steel substrate resulted in a reduction of the corrosion current by 85% concerning the substrate material. Such a significant improvement in corrosion resistance results from the fact that the nanoTiO_2 layer with amorphous structure features obtained with the ALD technique tightly covers all structural defects of the TiO_2 coating obtained with the PVD technique. The authors propose to use a similar barrier to the development of corrosion in the case of the Al-Si-Cu alloy substrate. Therefore, the presented work aims to investigate the effect of coating the Al-Si-Cu aluminium alloy substrate with a hybrid bimodal TiO_2/nanoTiO_2 coating and to relate these test results to the tests of the same phases obtained separately on this substrate.

2. Materials and Methodology

2.1. Sample Preparation

The tests were carried out on Al-Si-Cu-type aluminium alloys heat-treated by precipitation hardening. Samples made of alloys with a diameter of 14 mm and a height of about 5 mm were mechanically polished on papers and discs with decreasing gradation. After each step, the media were rinsed in an ultrasonic bath with acetone and isopropanol and then dried with a blast of hot air. The tests were performed on uncoated substrate materials and those covered with TiO_2, nanoTiO_2 coatings, and a bimodal TiO_2/nanoTiO_2 coating, obtained using PVD, ALD, and the PVD/ALD hybrid process, respectively.

The reactive magnetron sputtering method was used to deposit the TiO_2-type PVD coating (Kurt J Lesker PVD 75 device, Clairton, PA, USA), in which a pure titanium target was used as the source of the titanium vapour. Two gases were used in the process: argon and oxygen, as the reactive gas. The deposition was carried out at a temperature of 100 °C with a constant current vapour source. The magnetron power used was 200 W, and the bias voltage of the BIAS substrate was 140 V. First, a pure titanium sublayer was deposited and sputtered for 2 min under a pure Argon atmosphere. Then, the titanium oxide layer was deposited for 120 min. The thickness of the coating obtained in this way was about 120 nm.

The titanium oxide nano-coating TiO_2 was deposited by the atomic deposition of ALD layers using a Picosun ALD R-200 reactor with thermal excitation. The source of titanium was the $TiCl_4$ precursor, while the source of oxygen was water. The times for dosing the precursor ($TiCl_4$) and the reagent (H_2O) were the same and amounted to 0.1 s. The chamber was purged with pure nitrogen for 4 s after the precursor and 5 s after water. The thickness of the coating obtained in this way was about 16 nm.

The bimodal coating of the TiO_2/nanoTiO_2 type was obtained by coating the substrate successively, first by the PVD process and then by the ALD process according to the above procedures.

2.2. Characterisation

The morphology of coatings and surfaces was examined on a Zeiss Supra 35 scanning electron microscope(Zeiss, Oberkochen, Germany), equipped with the EDS detector made by Thermo Scientific. This examination was performed after corrosion and tribological tests.

The detection of secondary electrons (SE) was used for imaging the examined surfaces. The applied accelerating voltage was in the range of 5–20 kV.

The atomic force microscope (Park Systems XE-100, Suwon, Korea) was used to study the morphology of the coatings. AFM measurements were performed in a non-contact mode, examining the areas of 10 μm × 10 μm and 1 μm × 1 μm.

Both potentiodynamic and EIS methods were used to determine the corrosion resistance of the samples, employing the potentiostat-galvanostat ATLAS 0531 EU&IA. DC tests were carried out in the vessel and three-electrode systems in the 3.5% NaCl solution environment. A saturated silver-plated electrode was used as the reference electrode, while a platinum plate was the auxiliary electrode.

During the tests, the θ contact angle was measured by the sessile drop method to determine the nature of the chemical structure of the tested samples' surfaces. The measurement system was used, consisting of the Surtens Universal goniometer (OEG, Frankfurt, Germany), equipped with a camera for taking pictures of drops of the measure liquids, and a computer with Surtens 4.5 Software, used to analyse the recorded images. The liquids used for the research were polar liquid and dispersion liquid. The calculation of the free surface-free energy (SFE) (γ^S) and its components, i.e., polar ($\gamma_p{}^S$) and dispersive ($\gamma_d{}^S$), was performed using the Owens–Wendt method.

The wear resistance tests were performed on a CSM Instruments tribometer (Anton Paar, Peseux, Switzerland) in the ball-on-disc mode in the air atmosphere at room temperature. The WC-Co balls with 6 mm diameter were used as counter-samples. Testing parameters were as follows: wear diameter 5 mm, linear speed v = 0.5 cm/s, and normal force Fn = 0.5 N. The friction coefficient was recorded as a function of the number of cycles during the test. The investigations were performed up to the maximum number of cycles—500 (the cycle is equal to a complete revolution of the sample).

3. Results and Discussion

Examination of the morphology of the coatings with the use of AFM (Figure 1) showed that there were minor scratches on the surface of the tested materials, which are undoubtedly a remnant of the process of mechanical preparation of the substrate for coating. The small thickness of these coatings, ranging from about 16 nm for ALD layers to about 136 nm for bimodal coatings, makes them reproduce the morphology of the substrate on which they are applied. Moreover, the PVD coating and the bimodal coating consist of nanostructured grains with a size of about 1–3 nm (Figures 1a,c and 2a). The TiO_2 coating obtained with the ALD technique did not show such grains, which may indicate its amorphous structure.

Table 1 shows the Sa roughness parameters obtained as a result of the morphology of the samples. An AFM microscope was used for the study. Based on the performed tests, it was found that the roughness (S_a) was in the order of 1.9 to 3.4, from 6.1 to 7.4 nm, for the area of 1 and 100 μm^2. With the increase in the test area, the trend was maintained, despite the increase in the roughness parameter. This should be understood as the situation where the deposited coatings contribute to a slight smoothing of the surface with the uncoated substrate. It should be emphasised that we are talking about roughness on a very small scale, actually the nanoscale.

Moreover, the chemical composition analysis from the surface of the coatings confirmed the presence of titanium and oxygen, suitable for the obtained coatings (Figure 2b). The EDS spectrograms also showed reflections from aluminium, which is the main component of the substrate, due to the small thickness of the coatings, much smaller than the emission depth of the characteristic X-rays.

Cross-sectional thin-film testing of the PVD/ALD hybrid coating showed that the coating consists of three layers (Figures 3 and 4). The PVD bilayer consists of a titanium sublayer and a titanium oxide-specific layer. Diffraction analysis confirmed that TiO_2-PVD layers show a crystalline structure. This layer has a tetragonal structure belonging to the $P4_2/mnm$ space group (rutile). The rutile phase is formed in the MSPVD coatings, despite the relatively low temperature of the deposition process under specific process conditions,

particularly with high magnetron power. Reference [34] contains similar dependencies. The titanium oxide layer obtained on the surface of the tested materials by the ALD method shows an amorphous structure, as evidenced by a slightly blurred microscopic image from this area (Figure 3b), characteristic of this type of atomic structure.

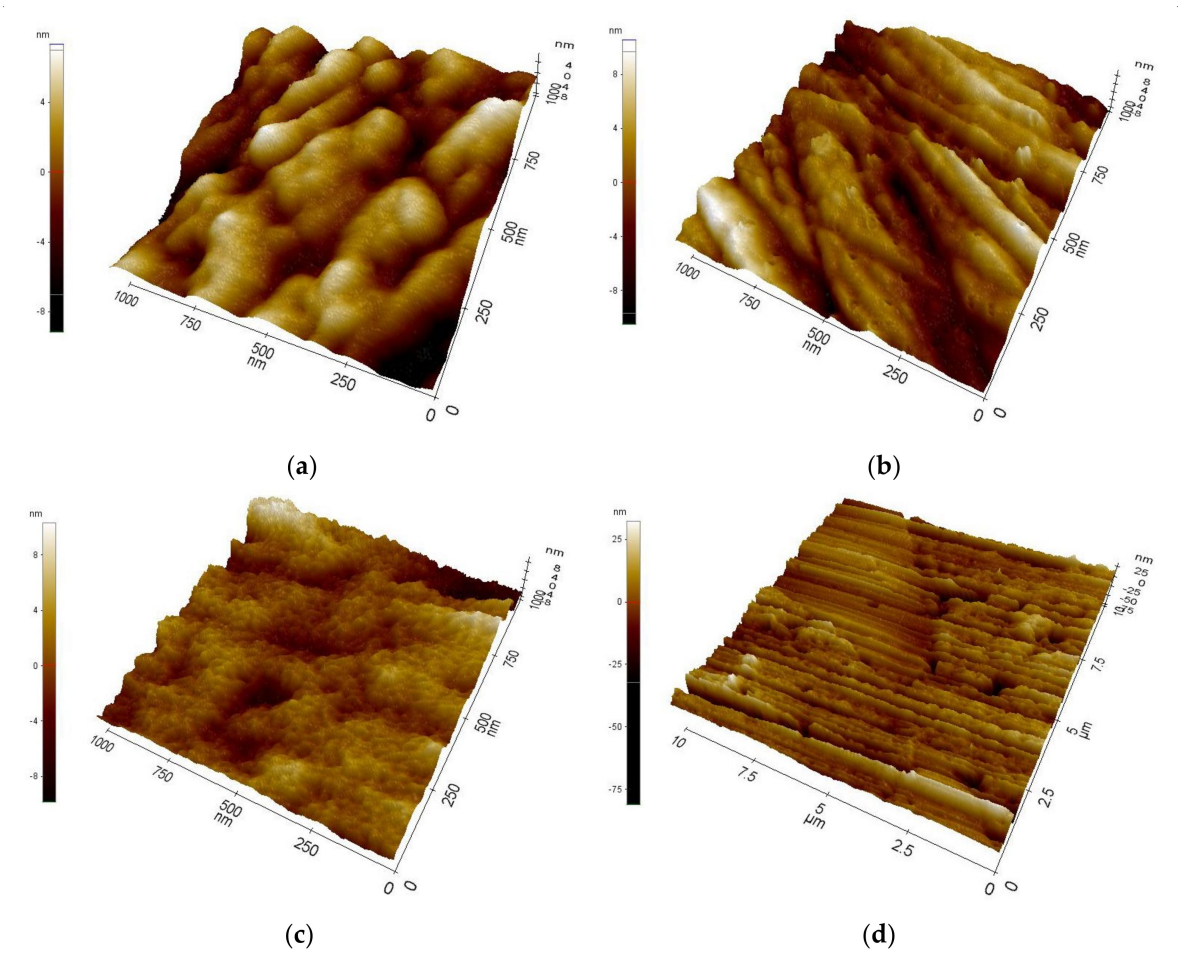

Figure 1. Morphology of investigated coatings on Al-Si-Cu alloy substrate obtained by: (**a**) PVD (1 × 1 µm AFM image), (**b**) ALD (1 µm × 1 µm AFM image), (**c**) hybrid PVD/ALD (1 µm × 1 µm AFM image), and (**d**) hybrid PVD/ALD (10 µm × 10 µm AFM image).

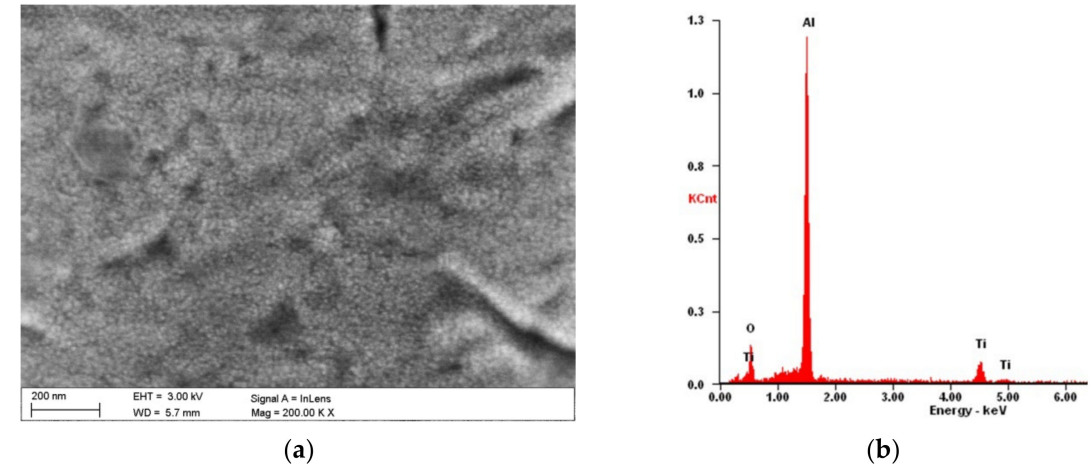

Figure 2. Morphology of TiO_2/nanoTiO_2 bimodal coating on Al-Si-Cu alloy substrate: (**a**) SEM image and (**b**) X-ray energy-dispersive plot of the area shown in (**a**).

Table 1. The surface roughness of the investigated materials was obtained using an AFM microscope.

Coating	Roughness S_a (nm) AFM Area	
	1 μm × 1 μm	10 μm × 10 μm
uncoated	3.4	7.4
TiO_2 (PVD)	2.6	6.5
nanoTiO_2 (ALD)	2.2	6.1
TiO_2/nanoTiO_2 (PVD/ALD)	1.9	6.3

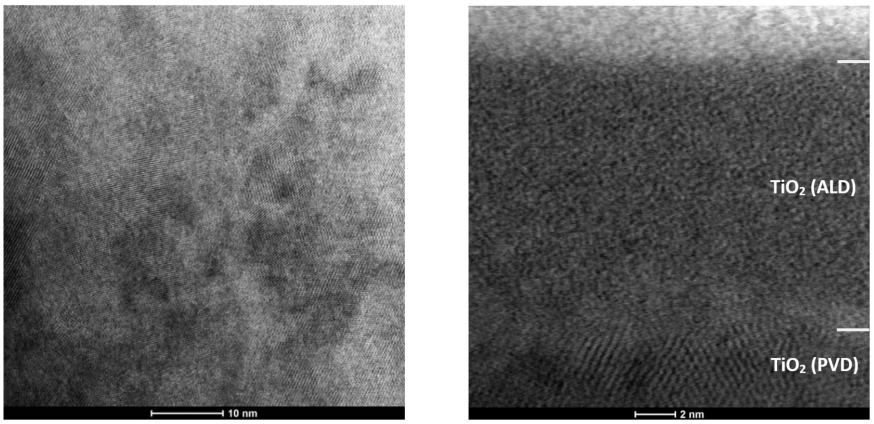

(**a**) (**b**)

Figure 3. Structure (STEM) of TiO_2/TiO_2 bimodal coating: (**a**) structure of TiO_2 (PVD) layer and (**b**) structure of TiO_2 (ALD) layer and PVD/ALD transition zone.

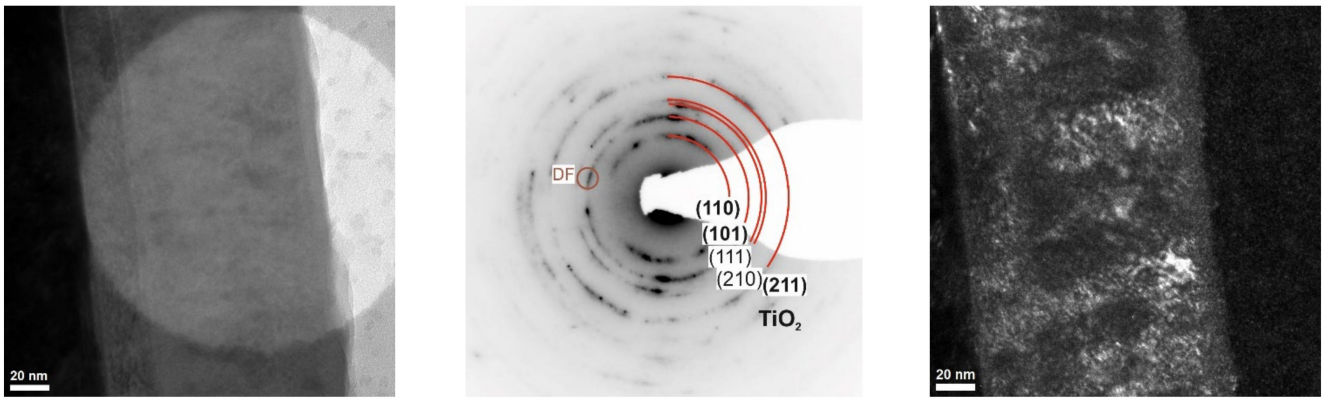

(**a**) (**b**) (**c**)

Figure 4. Structure (TEM) of TiO_2/TiO_2 bimodal coating obtained: (**a**) bright-field—an area of diffraction analysis, (**b**) diffraction pattern, and (**c**) dark field from reflections corresponding to the planes (101) for the TiO_2 phase.

Corrosion resistance was determined based on potentiodynamic tests. The open-circuit potential was determined without current conditions. Then, the potentiodynamic curves of the cathodic and anodic polarisation were recorded (Figure 5) and, based on the Tafel analysis, the values of the corrosion potential (E_{corr}), the corrosion current density (j_{corr}), and the polarisation resistance (R_{pol}) were determined. The obtained values are summarised in Table 2. As a result of the research, it was found that, as assumed, the bimodal hybrid coating TiO_2/nanoTiO_2 had the highest corrosion resistance. The polarisation resistance value for this coating was the highest, almost R_{pol} = 730 kΩ cm^2, and the current density was the lowest, with a value of j_{corr} = 0.007 μA/cm^2. For comparison, the polarisation resistance

of both the uncoated substrate and the substrate covered with the TiO_2 PVD coating was two orders of magnitude lower, and in both cases, it was about $R_{pol} \approx 4.5$ kΩ cm^2, while the value for the uncoated substrate was slightly higher. The current density for the substrate and PVD coating was three orders of magnitude higher than the bimodal coating and oscillated around the value of $j_{corr} \approx 2.4$ μA/cm^2. The values characterising the corrosion resistance of the ALD coating show a higher corrosion resistance than the PVD coating and the uncoated substrate, but much lower than the PVD/ALD hybrid coating. Moreover, as a result of morphology studies using the SEM of samples after corrosion tests, the effect of coatings on reducing corrosion pitting was confirmed (Figure 6).

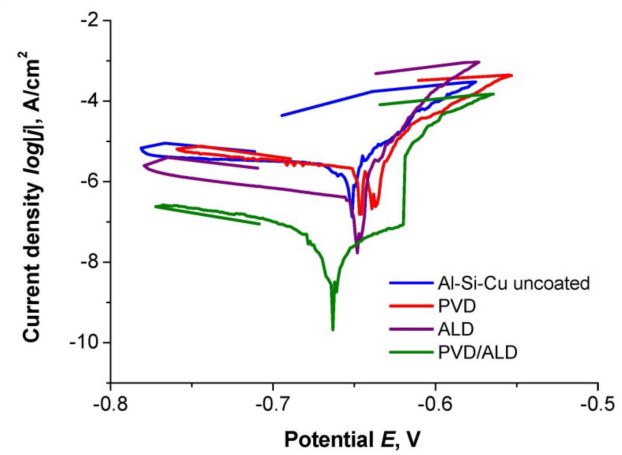

Figure 5. Anodic polarisation curves for an uncoated Al-Si-Cu alloy substrate, as well as coated by the investigated coatings.

Table 2. Summary of corrosion parameter values from Tafel analysis of investigated samples.

Coating	E_{corr} (V)	j_{corr} (A/cm^2)	R_{pol} (Ω·cm^2)
uncoated	-650×10^{-3}	2.68×10^{-6}	4.73×10^3
TiO_2 (PVD)	-639×10^{-3}	2.06×10^{-6}	4.37×10^3
nanoTiO_2 (ALD)	-648×10^{-3}	0.38×10^{-6}	14.20×10^3
TiO_2/nanoTiO_2 (PVD/ALD)	-662×10^{-3}	0.007×10^{-6}	729.92×10^3

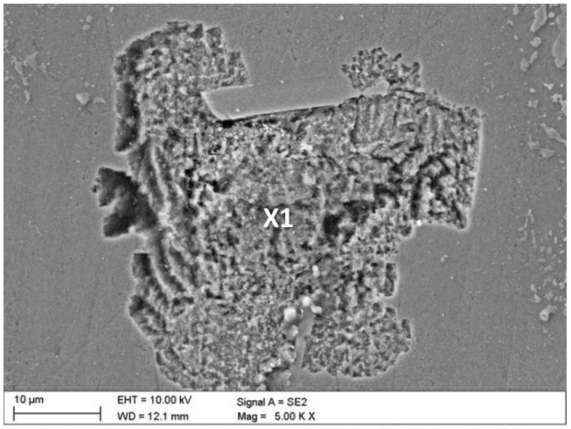

(**a**)

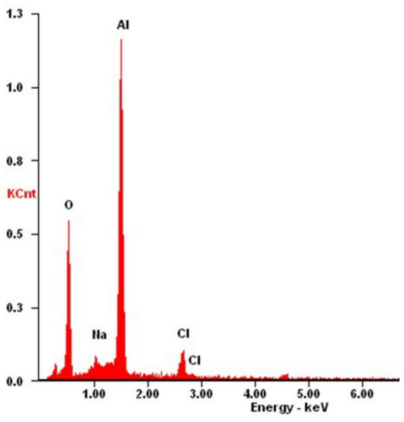

(**b**)

Figure 6. Morphology after an electrochemical examination of the sample coated by the nanoTiO_2 ALD coating: (**a**) SEM image and (**b**) X-ray energy-dispersive plot of the area X1 shown in (**a**).

The study of electrochemical properties by the EIS method consisted of testing the system's response at the determined free potential (−65 mV) and the set frequency, in the form of a current impulse with amplitude minus the sample resistance, and the phase shifted with the excitation impulse. The frequency range used in the study varied from 100 kHz to 1 MHz. The results of the impedance measurements are presented in the form of Nyquist (Figure 7) and Bode (Figure 8) plots.

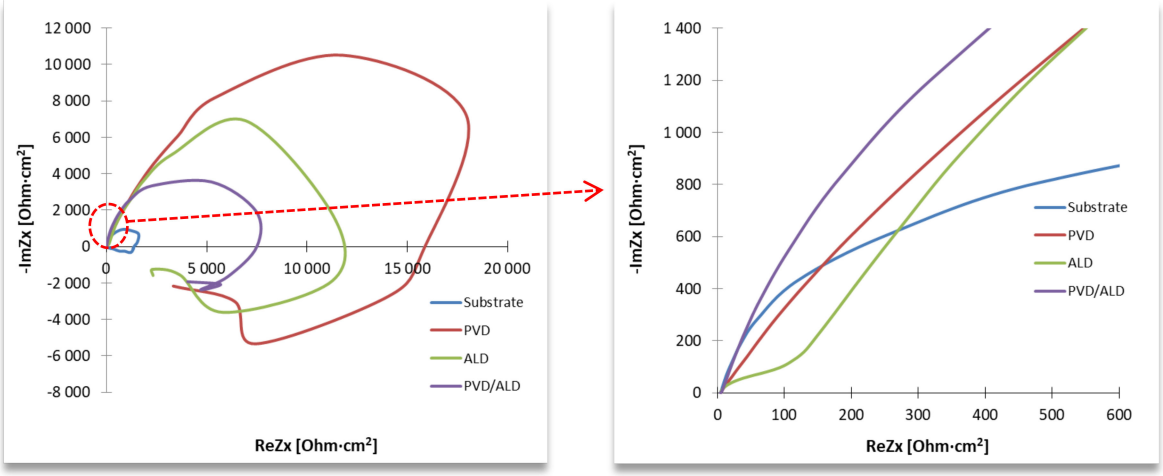

Figure 7. Impedance spectrum of the tested materials (for designated stationary potentials)—Nyquist representation: (**a**) full view, (**b**) limited view according to (**a**).

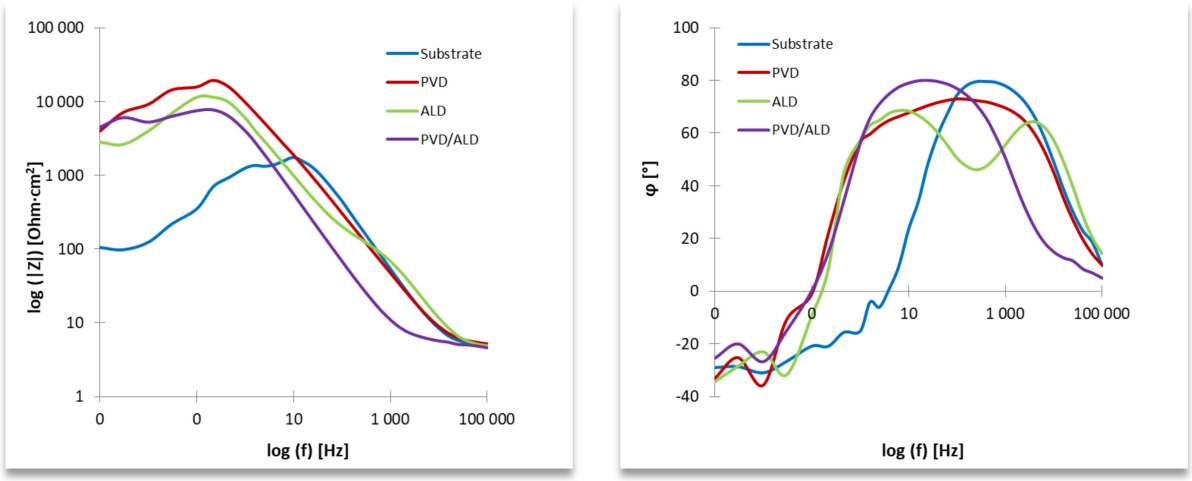

Figure 8. Impedance spectrum of the tested materials (for designated stationary potentials)—Bode representation: (**a**) impedance as a function of frequency and (**b**) phase angle as a function of frequency.

The course of the experimental curves with the curves generated by the computer model were compared to fit the equivalent electrical system to the obtained impedance spectra. A replacement circuit was selected. The equivalent circuit consists of three branches. The first two contain the constant phase element and a resistive element. The third branch consists of a combined inductor and a resistor since the fragment with a return arc in the low-frequency range is recorded in the Nyquist plot. This system reflected the resistance

of the surface layer of the material and the electrical resistance of the tested electrolyte (Figure 9), and its resultant impedance can be written following Equation (1).

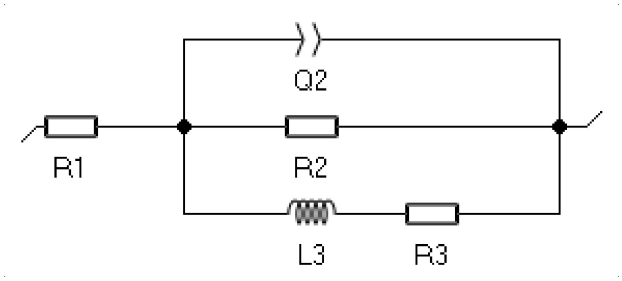

Figure 9. An equivalent circuit representing the impedance spectra of the investigated materials.

Based on the recorded results of protective coatings (in the form of a Nyquist and Bode diagram), it was found that the material had better anti-corrosion properties than the uncoated material sample. It was proven by the obtained value of the resistance of the element R_2 and the more exponential shape of the impedance spectrum in the Nyquist diagram, which is visible in the range from high- to medium-frequency values between 100 kHz and 1 Hz. Based on the analysis of the full spectrum of the Nyquist diagram and the shape of the registered semicircles of the obtained coatings, we can find that low porosity is a characteristic of these coatings.

$$Z = R_1 + \frac{R_2 \cdot (L_3 j2\pi f + R_3)}{R_2 + (L_3 j2\pi f + R_3) + R_2 \cdot Y_2 (j2\pi f)^{n2} \cdot (L_3 j2\pi f + R_3)} \quad (1)$$

Table 3 shows the calculation results matching the experimental ones, and these are the parameters of the elements of the adopted equivalent circuit.

Table 3. Electrical equivalent circuit values of the investigated materials.

Coating	R1 (Ω)	Y2 ($F \cdot s^{(n2-1)}$)	n2	R2 ($k\Omega \cdot cm^2$)	L3 (kH)	R3 ($k\Omega \cdot cm^2$)
uncoated	4.7	4.82	0.945	1.5	0.5	0.3
TiO_2 (PVD)	4.8	7.19	0.907	22	10	5.2
nanoTiO_2 (ALD)	3.3	53.0	0.685	20	34	3.2
TiO_2/nanoTiO_2 (PVD/ALD)	5.1	32.19	0.937	8.3	95	8.9

The results of the impedance measurements recorded in the form of Bode diagrams allow stating that with the increase of the frequency of the excitation signal, the impedance module of the tested system decreased.

Moreover, the analysis of Bode diagrams allows us to state that, compared with the base material, all types of applied coatings slowed down the corrosion processes for the tested material in the range from high- to medium-frequency values (Figure 8). Moreover, comparing the effectiveness of the applied coating systems based on Bode diagrams, it can be observed by practically the entire frequency range used in the tests that the lowest values of the impedance modulus occurred for the PVD/ALD coating.

In the case of all applied coatings on samples of the base material, the determined values of the *n* coefficient of the CPE element were close to 0, which makes it possible to determine their resistive nature.

The recorded maximum values of the phase-shift angle in the tested equivalent systems were 73° for the PVD coating at a frequency of 100 Hz, 69° for the ALD coating at the frequency of 6.3 Hz, and 80° for the PVD/ALD coating at 25 Hz, which was the highest value, and these may show less tendency to form a porous corrosion layer.

The measurement results of the surface contact angles of the tested materials and the determined surface-free energy (SFE) are summarised in Table 4. Figure 10 presents exemplary images of water droplets and diiodomethane on the surface of the tested TiO_2/nanoTiO_2 hybrid coating and plots of the contact angle as a function of time. As a result of the study, it was found that the values of the water contact angles of the surface of the uncoated aluminium alloy and that coated with the TiO_2/nanoTiO_2 hybrid coating were similar and amounted to 86° and 81°, respectively. It proves that these surfaces are hydrophilic, and the deposition of a hybrid coating increases the hydrophilicity. However, in the case of PVD and ALD coatings, the values of the angle θ were the same and amounted to 95°, which proves the hydrophobicity of these surfaces. The values of diiodomethane contact angles for all tested samples were similar and fell within the range of 53°–61°. Moreover, it was found that the surface-free energy values were similar and fell within 29–34 mJ/m^2. For all tested materials, the components of non-polar SFE values were much greater than the polar components, proving that all tested materials showed a higher affinity for the dispersion groups of SFE.

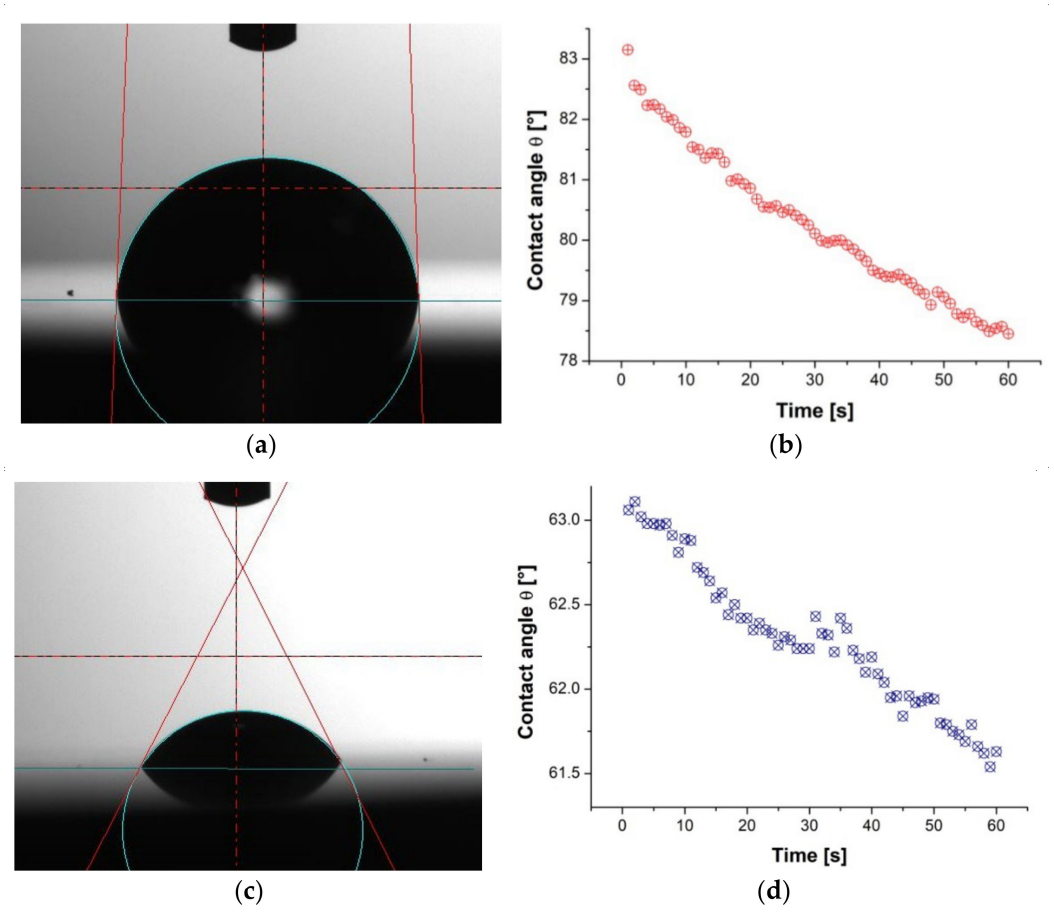

Figure 10. Results of contact angle measurements of the TiO_2/nanoTiO_2 hybrid coating: (**a**) water drop, (**b**) contact angle value changes as a function of time for water, (**c**) diiodomethane drop, and (**d**) contact angle value changes as a function of time for diiodomethane.

Table 4. The contact angle measurements and the surface energy calculated by the Owens–Wendt method.

Coating	Wetting Angle (°)		Surface-Free Energy (mJ/m^2)		
	Distilled Water	Diiodomethane	$\gamma_p{}^S$	$\gamma_d{}^S$	γ_S
uncoated	86 ± 3	56 ± 2	4	27	31
TiO_2 (PVD)	95 ± 3	59 ± 1	1	29	30
nanoTiO_2 (ALD)	95 ± 4	53 ± 2	1	33	34
TiO_2/nanoTiO_2 (PVD/ALD)	81 ± 4	61 ± 2	9	20	29

The results of the tribological tests include the recorded coefficients of friction, μ, as a function of the number of cycles (Figure 11) and microscopic observations of the wear and counter-samples' paths (Figure 12). The coefficient of friction of the friction pair of aluminium alloy-cemented carbides (counter-sample) was approximately 0.5 and closely corresponds to the literature value. The registered friction coefficients for the tested TiO_2 coatings in the initial test cycles had low values of μ, below 0.2. After a certain number of cycles, the coefficient usually increases rapidly, proving that the thin test coating has worn through and the aluminium substrate is exposed. The number of cycles at which the coating is rubbed to the substrate is the so-called Cycles critical (C_c). These values equalled 37, 83, and 168 for ALD, PVD, and hybrid PVD/ALD coatings, respectively.

Based on the observation of the abrasion paths in the scanning electron microscope, it was found that the primary mechanism of the resulting damage was abrasion (Figure 12). As a result of abrasion, the substrate was exposed, and the surface was oxidised. In addition, tensile damage to the coating was found at the edge of the cracks (Figure 12b). Accumulation of oxidised aluminium was found on the surface of the counter-sample, which was confirmed by EDS analysis (Figure 12c,d). On the other hand, the traces of wear on the sintered carbide shanks were slight and hardly noticeable.

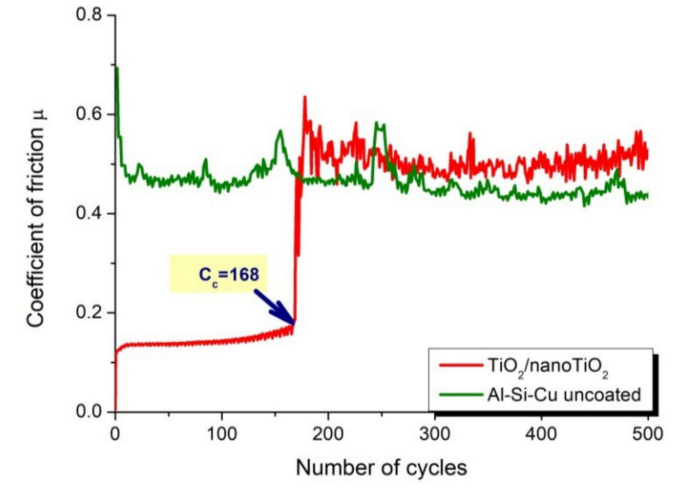

Figure 11. Friction coefficient as a function of the number of cycles for the uncoated Al-Si-Cu alloy substrate material and the TiO_2/nanoTiO_2 coating obtained by a hybrid method.

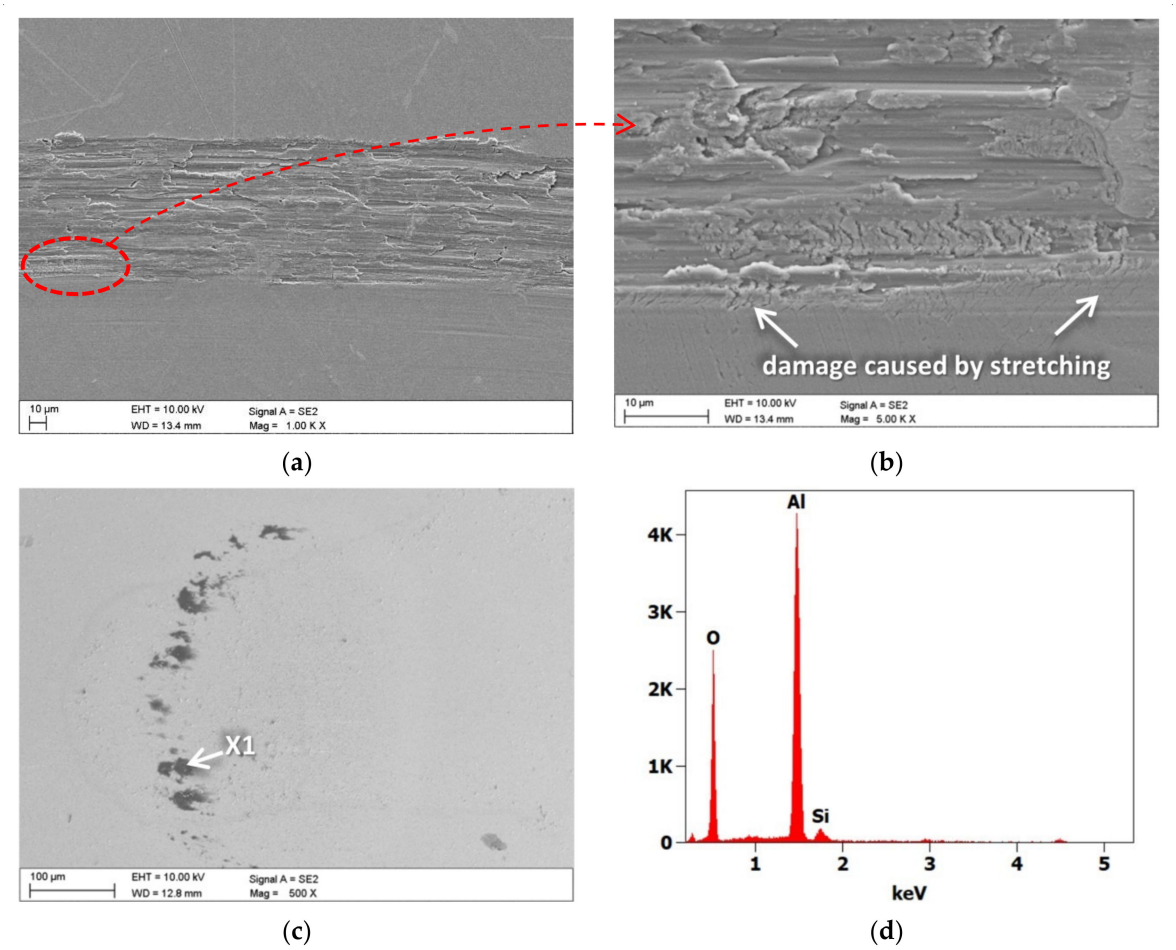

Figure 12. (**a**,**b**) Wear trace after the "ball-on-disc" wear test for TiO_2/nanoTiO_2 bimodal coatings, (**c**) wear place after the "ball-on-disc" wear test for cemented carbide ball as a counter-sample, and (**d**) X-ray energy dispersive plot of the area X1 in (**c**).

4. Summary

Aluminium alloys combine such features as low density and high strength, and relatively high corrosion resistance, thanks to which they are, after steel, the most commonly used construction material. Therefore, ensuring a high pace of development in the field of material technology of aluminium alloys has become of interest in both scientific and industrial environments.

Chemical modification and shaping of the structure and surface layer properties can be performed by developing engineering materials (including aluminium alloys). Traditional surface treatment technologies are more and more often being replaced by hybrid technologies, which, thanks to the combination of two or more treatment methods, allow for obtaining material properties through the synergy that cannot be achieved with any other methods. This paper presented the results of tests of a TiO_2/nanoTiO_2 coating, which was called a bimodal coating, because it consists of two layers of the same type, i.e., titanium oxide (excluding the Ti sublayer) obtained in a hybrid process consisting of two separate PVD and ALD technologies. As shown by the structural studies with the use of the scanning transmission microscope, the structure of such a bimodal coating consists of a crystalline TiO_2 layer, with a crystalline Ti sublayer obtained in the MS-PVD process and an amorphous nanoTiO_2 layer as the last layer obtained by the ALD technique. As a result of studies using the potentiodynamic method and electrochemical impedance spectroscopy (EIS), it was found that the tested hybrid coating on the Al-Si-Cu alloy substrate showed much higher electrochemical properties compared to titanium oxide coatings obtained in single PVD and ALD processes. Moreover, it was found that titanium

oxide obtained by the PVD method did not improve the anti-corrosion properties among the single tested coatings, and the ALD technology obtained improved anti-corrosion properties, however to a much lesser extent than the tested hybrid coating (Table 2 and Figure 13). Similar relationships of titanium oxide coatings obtained by the PVD, ALD, and PVD/ALD processes on the substrate made of 316 L austenitic steel were found in [27]. The low anti-corrosion properties of the TiO_2 coating deposited with the PVD method should undoubtedly be associated with its crystalline structure and possible microstructural defects of these types of coatings [28,29].

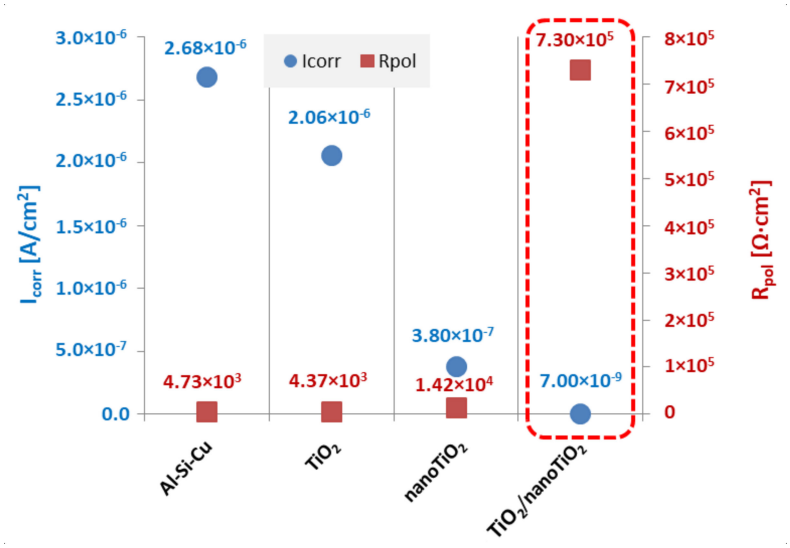

Figure 13. Summary of corrosion parameters' values from Tafel analysis of investigated samples in 3.5% NaCl solution.

As a result of tribological tests, it was found that the tested coatings reduced the friction coefficient concerning the uncoated Al-Si-Cu substrate. Moreover, it was found that hybrid coatings exhibited the highest abrasion resistance. Cycles critical (C_c), which is a measure of abrasion resistance, is in this case convergent with the thickness of the tested coatings, where the ALD coating had the smallest thickness, and the hybrid coating had the largest. It should be noted that, as in the case of corrosion resistance, there was a synergistic reinforcement effect in the case of abrasion resistance. This is evidenced by the fact that the abrasion resistance expressed by the C_c value of the bimodal TiO_2/nanoTiO_2 hybrid coating (C_c = 168) was greater than the sum of the Cycles critical values for PVD (C_c = 83) and ALD (C_c = 37) coatings.

Similar abrasion resistance results for this type of bimodal titanium oxide coating on an austenitic steel substrate are presented in [27]. The influence of the tested coatings on wettability and surface-free energy was small. The measurements of the wettability angle (Table 4) showed that the uncoated surface and the hybrid coating have hydrophilic properties, and the PVD and ALD coatings are hydrophobic—all the properties of the contact angle Θ for distilled water oscillated around the value of 90°. The small influence of the coatings on this value is evidenced by the SFE differences, which were small.

Summing up, it should be emphasised that the main feature of the TiO_2/nanoTiO_2 PVD+ALD hybrid bimodal coatings is the increased corrosion resistance of the coated Al-Si-Cu substrates. Of course, comparing them to the uncoated substrate and the titanium oxide coatings produced by single PVD and ALD processes, the obtained tribological properties are typical for these types of thin nanometric oxide coatings.

The results presented in this paper may constitute a proposal for a technological solution to be used, inter alia, for utility elements such as fittings or interior finishing elements. On the other hand, these studies may constitute the basis for further development

of hybrid coatings towards increasing the electrochemical and mechanical properties of light metal alloys coated with them.

5. Conclusions

Based on the research results, it was found that:

- The highest corrosion resistance was demonstrated by bimodal TiO_2/nanoTiO_2 coatings, which was obtained thanks to the synergistic interaction of two titanium oxide layers obtained in a process combining PVD and ALD methods.
- The corrosion current density of the bimodal coating was three orders of magnitude lower compared to the uncoated substrate and PVD coating, and two orders of magnitude lower than that of the ALD coating.
- All tested oxide coatings reduced the friction coefficient, μ, by a value of approximately 0.3 compared to the substrate without a coating, with the highest durability expressed in the C_c for hybrid coatings, the number of C_c of which was higher than the sum of C_c for PVD and ALD coatings.

Author Contributions: Conceptualisation, M.S.; methodology, M.S., D.P., Ł.R., M.P. and P.C.; investigation, M.S., D.P., Ł.R., M.P., P.C., M.M.-S. and P.B.; interpretation of data, M.S., D.P., Ł.R., M.P., P.C., M.M.-S. and P.B.; data curation, M.S.; writing—original draft preparation, M.S., D.P., Ł.R., M.P., P.C., M.M.-S. and P.B.; writing—review and editing, M.S., D.P., Ł.R., M.P., P.C., M.M.-S. and P.B.; visualisation, M.S. and D.P.; supervision, M.S.; project administration, M.S.; funding acquisition, M.S. and D.P. All authors have read and agreed to the published version of the manuscript.

Funding: This research received no external funding.

Institutional Review Board Statement: Not applicable.

Data Availability Statement: The data presented in this study are available upon request from the corresponding author.

Conflicts of Interest: The authors declare no conflict of interest.

References

1. Labisz, K. Structure and properties of the casting surfaces Al-Si-Cu. *Open Access Libr.* **2013**, *5*, 1–152. (in Polish).
2. Białobrzeski, A.; Czekaj, E.; Heller, M. Corrosion properties of aluminum and magnesium alloys processed by pressure die casting technology. *Arch. Foundry* **2002**, *2*, 294–313. (in Polish).
3. Przybyłowicz, K. *Metaloznawstwo*; WNT: Warsaw, Poland, 2007. (in Polish)
4. Tański, T.; Wiśniowski, M.; Matysiak, W.; Staszuk, M.; Szklarek, R. Surface treatment of heattreated cast magnesium and aluminium alloys. *Mater. Technol.* **2016**, *50*, 699–706.
5. Staszuk, M.; Pakuła, D.; Chladek, G.; Pawlyta, M.; Pancielejko, M.; Czaja, P. Investigation of the structure and properties of PVD coatings and ALD plus PVD hybrid coatings deposited on sialon tool ceramics. *Vacuum* **2018**, *153*, 184–190. [CrossRef]
6. Staszuk, M.; Pakuła, D.; Tański, T. Investigation studies involving wear resistant ALD/PVD hybrid coatings on sintered tool substrate. *Mater. Tehnol.* **2016**, *55*, 755–759. [CrossRef]
7. Dobrzański, L.A.; Pakuła, D.; Mikuła, J.; Gołombek, K. Investigation of the structure and properties of coatings deposited on ceramic tool materials. *Int. J. Surf. Sci. Eng.* **2007**, *1*, 111–124. [CrossRef]
8. Shan, C.X.; Hou, X.; Choy, K.-L. Corrosion resistance of TiO_2 films grown on stainless steel by atomic layer deposition. *Surf. Coat. Technol.* **2008**, *202*, 2399–2402. [CrossRef]
9. Basiaga, M.; Walke, W.; Staszuk, M.; Kajzer, W.; Kajzer, A.; Nowińska, K. Influence of ALD process parameters on the physical and chemical properties of the surface of vascular stents. *Arch. Civ. Mech. Eng.* **2017**, *17*, 32–42. [CrossRef]
10. Díaz, B.; Härkönen, E.; Światowska, J.; Seyeux, A.; Maurice, V.; Ritala, M.; Marcus, P. Corrosion properties of steel protected by nanometre-thick oxide coatings. *Corros. Sci.* **2014**, *82*, 208–217. [CrossRef]
11. Fedel, M.; Deflorian, F. Electrochemical characterization of atomic layer deposited Al_2O_3 coatings on AISI 316L stainless steel. *Electrochim. Acta* **2016**, *203*, 404–415. [CrossRef]
12. Marin, E.; Guzman, L.; Lanzutti, A.; Ensinger, W.; Fedrizzi, L. Multilayer Al_2O_3/TiO_2 Atomic Layer Deposition coatings for the corrosion protection of stainless steel. *Thin Solid Film.* **2012**, *522*, 283–288. [CrossRef]
13. Walke, W.; Kaczmarek, M.; Staszuk, M.; Basiaga, M. Influence of purge, time of waiting and TiCl4 dosing time in a low-pressure atomic layer deposition (ALD) reactor on properties of TiO_2 layer. *Metalurgija* **2017**, *56*, 179–181.
14. Basiaga, M.; Staszuk, M.; Walke, W.; Tański, T.; Kajzer, W. Potentiostatic, potentiodynamic and impedance study of TiO_2 layers deposited of 316 LVM steel used for coronary stents. *Arch. Metall. Mater.* **2016**, *61*, 821–824. [CrossRef]

15. Müller, B.; Haugen, H.; Nilsen, O.; Tiainen, H. Atomic layer deposited TiO_2 protects porous ceramic foams from grain boundary corrosion. *Corros. Sci.* **2016**, *106*, 35–42. [CrossRef]
16. Hendricks, O.L.; Tang-Kong, R.; Babadi, A.; McIntyre, P.C.; Chidsey, C. Atomic layer deposited TiO_2-IrOx alloys enable corrosion resistant water oxidation on silicon at high photovoltage. *Chem. Mater.* **2019**, *31*, 90–100. [CrossRef]
17. Zhu, C.; Ma, F.; Dai, Z.; Ma, D. Atomic Layer Deposition of TiO_2 thin films on the inner walls of steel tubes increases anti-coking properties. *ACS Omega* **2020**, *5*, 32102–32111. [CrossRef]
18. Aarika, L.; Kozlova, J.; Mändar, H.; Aarik, J.; Sammelselg, V. Chemical resistance of TiO_2 and Al_2O_3 single-layer and multilayer coatings atomic layer deposited from hydrogen-freeprecursors on silicon and stainless steel. *Mater. Chem. Phys.* **2019**, *228*, 285–292. [CrossRef]
19. Mirhashemihaghighi, S.; Światowska, J.; Maurice, V.; Seyeux, A.; Zanna, S.; Salmi, E.; Ritala, M.; Marcusa, P. Corrosion protection of aluminium by ultra-thin atomic layer deposited alumina coatings. *Corros. Sci.* **2016**, *106*, 16–24. [CrossRef]
20. Radi, P.A.; Testoni, G.E.; Pessoa, R.S.; Maciel, H.S.; Rocha, L.A.; Vieira, L. Tribocorrosion behavior of TiO_2/Al_2O_3 nanolaminate, Al_2O_3, and TiO_2 thin films produced by atomic layer deposition. *Surf. Coat. Technol.* **2018**, *349*, 1077–1082. [CrossRef]
21. Gonullu, M.P.; Ates, H. Investigation of the impact of annealing on the structural, optical and morphological evolution of mixture-phase ALD-TiO_2 films containing brookite. *Superlattices Microstruct.* **2020**, *147*, 106699. [CrossRef]
22. Chung, H.K.; Won, S.O.; Park, Y.; Kim, J.-S.; Park, T.J.; Kim, S.K. Atomic-layer deposition of TiO_2 thin films with a thermally stable (CpMe5)Ti(OMe)3 precursor. *Appl. Surf. Sci.* **2021**, *550*, 149381. [CrossRef]
23. Basiaga, M.; Kajzer, W.; Walke, W.; Kajzer, A.; Kaczmarek, M. Evaluation of physicochemical properties of surface modified Ti6Al4V and Ti6Al7Nb alloys used for orthopedic implants. *Mater. Sci. Eng. C* **2016**, *68*, 851–860. [CrossRef] [PubMed]
24. Lagrange, M.; Sannicolo, T.; Muñoz-Rojas, D.; Lohan, B.G.; Khan, A.; Anikin, M.; Jiménez, C.; Bruckert, F.; Bréchet, Y.; Bellet, D. Understanding the mechanisms leading to failure in metallic nanowire-based transparent heaters, and solution for stability enhancement. *Nanotechnology* **2016**, *28*, 055709. [CrossRef] [PubMed]
25. Johnson, R.W.; Hultqvist, A.; Bent, S.F. A brief review of atomic layer deposition: From fundamentals to applications. *Mater. Today* **2014**, *17*, 236–246. [CrossRef]
26. Staszuk, M. Application of PVD and ALD Methods for Surface Treatment of Al-Si-Cu Alloys. *Solid State Phenom.* **2019**, *293*, 97–109. [CrossRef]
27. Marin, E.; Guzman, L.; Lanzutti, A.; Fedrizzi, L.; Saikkonen, M. Chemical and electrochemical characterization of hybrid PVD+ALD hard coatings on tool steel. *Electrochem. Commun.* **2009**, *11*, 2060–2063. [CrossRef]
28. Leppäniem, J.; Sippola, P.; Broas, M.; Aromaa, J.; Lipsanen, H.; Koskinen, J. Corrosion protection of steel with multilayer coatings: Improving the sealing properties of physical vapor deposition CrN coatings with Al_2O_3/TiO_2 atomic layer deposition nanolaminates. *Thin Solid Film.* **2017**, *627*, 59–68. [CrossRef]
29. Harkonen, E.; Kolev, I.; Díaz, B.; Światowska, J.; Maurice, V.; Seyeux, A.; Marcus, P.; Fenker, M.; Toth, L.; Radnoczi, G.; et al. Sealing of hard crn and dlc coatings with atomic layer deposition. *ACS Appl. Mater. Interfaces* **2014**, *6*, 1893–1901. [CrossRef]
30. Wan, Z.; Zhang, T.F.; Ding, J.C.; Kim, C.M.; Park, S.H.; Yang, Y.; Kim, K.H.; Kwon, S.H. Enhanced corrosion resistance of PVD-CrN coatings by ALD sealing layers. *Nanoscale Res. Lett.* **2017**, *12*, 248. [CrossRef]
31. Shan, C.X.; Hou, X.; Choy, K.L.; Choquet, P. Improvement in corrosion resistance of CrN coated stainless steel by conformal TiO_2 deposition. *Surf. Coat. Tech.* **2008**, *202*, 2147–2151. [CrossRef]
32. Leppaniemi, J.; Sippola, P.; Peltonen, A.; Aroma, J.J.; Lipsanen, H.; Koskinen, J. Effect of surface wear on corrosion protection of steel by CrN coatings sealed with Atomic Layer Deposition. *ACS Omega* **2018**, *3*, 1791–1800. [CrossRef] [PubMed]
33. Staszuk, M.; Pakuła, D.; Reimann, Ł.; Kloc-Ptaszna, A.; Pawlyta, M.; Kríž, A. Structure and properties of tio2/nanotio2 bimodal coatings obtained by a hybrid PVD/ALD method on 316L steel substrate. *Materials* **2021**, *14*, 4369. [CrossRef] [PubMed]
34. Lelis, M.; Tuckute, S.; Varnagiris, S.; Urbonavicius, M.; Laukaitis, G.; Bockute, K. Tailoring of TiO_2 film microstructure by pulsed-DC and RF magnetron cosputtering. *Surf. Coat. Tech.* **2019**, *377*, 124906. [CrossRef]